Check for updates

Effect of water content on the physical properties and structure of walnut oleogels†

Liqian Wang,[ab] Yuxiu Wen,[ab] Caihong Su,[ab] Yuan Gao,[ab] Qi Li,[ab] Shuangkui Du[ab] and Xiuzhu Yu [ID] *[ab]

This study aimed to investigate the effect of water content on the properties and structure of oleogels by developing walnut oleogel based on potato starch and candelilla wax (CW). Physical, thermal, rheological and microstructure characteristics of the walnut oleogel were determined by texture analyzer, differential scanning calorimeter, rotary rheometer, X-ray diffractometer and optical microscope. Results showed that with increased water content, the hardness of the oleogel increased from 123.35 g to 158 g, whereas the oil loss rate decreased from 24.64% to 10.91%. However, these two values decreased slightly when the ratio of oil to water was 1 : 1. The prepared oleogels have a high elastic modulus, and the flow behavior of all walnut oleogels conformed to that of a non-flowing fluid. Microstructure observation indicated that the crystal size and quantity increased with an increase in water content, and the liquid oil was wrapped in the crystal network by CW and potato starch, forming solidified droplets to further promote gelation. In conclusion, when the ratio of oil to water is 39%, the oleogel has good physical properties and stable crystal structure. These findings can provide an indication of water content in the composition of oleogels.

1. Introduction

Solid fats, such as partially hydrogenated vegetable oils and milk fats, are a major part of our daily diet due to their unique plastic and functional properties. However, conventional solid fats are usually rich in saturated and trans fatty acids, which may have negative effects on cardiovascular health and are associated with obesity and diabetes.[1,2] It is important to find an alternative that can replace these solid fat building blocks' functionalities, without any negative impact on health and quality. The research on oleogelation has attracted much attention among researchers for the development of healthy and structural fats. Oleogels are defined as gel systems.[3] They can be formed by supramolecular and minor gelator molecules, among others. Typical oleogels exhibit a solid-like, thermo-reversible, three-dimensional gel network and viscoelastic properties.[4–6] Considering the health and structural properties of oleogels, this material shows great application potential in the pharmaceutical, food, and cosmetics industry.[7]

The preparation process of oleogels requires gelling agents.[8] Marangoni and Garti (2011) found that the most promising food-grade gels are monoglycerides, waxes, lecithin and sorbitol tristearates, long-chain fatty acids, fatty alcohols,[9] protein, polysaccharides or their mixtures, phytosterols, and glutamate, because they are edible and can form stable oleogels. However, wax has many promising properties. For example, it can form a high oil-binding capacity and thermo-reversible oleogel at very low concentrations.[10] Meanwhile, a high concentration of wax may result in rougher waxy texture.

Recently, hydrocolloids have become very popular in the development of novel gel systems due to their excellent thickening, gelling and texture properties.[11] Silva et al. (2021) studied emulsion-filled hydrogels composed of potato starch (PS) and alginate, in which starch partially replaced alginate, thus changing the hydrogel network. It was reported that natural (sodium alginate) and synthetic (hydroxypropyl methylcellulose) polymer had been applied to develop a polymer-fish oil bigel (hydrogel/oleogel colloidal mixture). The results indicated that hydrogels are essential for the gel structure because of hydrogen bonding.[12] In addition, much research proved that methylcellulose and starch are promising hydrocolloid-based oleogelators in the food industry.[13–15] Potato starch is a main component of Chinese traditional staple food. Compared to other low-molecular-weight organogelators, PS is cheap, safe and healthy.[16–18] Besides, Zhai[19] et al. (2016) found that the addition of starch significantly affects the storage modulus of the emulsion during heating and cooling and increases the hardness, viscosity, and chewiness of the emulsion gel.

aCollege of Food Science and Engineering, Northwest A&F University, 22 Xinong Road, Yangling, Shaanxi, 712100, P. R. China. E-mail: xiuzhuyu@nwafu.edu.cn; Fax: +86-29-87092486; Tel: +86-29-87092308

bEngineering Research Center of Grain and Oil Functionalized Processing, Universities of Shaanxi Province, 22 Xinong Road, Yangling 712100, Shaanxi, P. R. China

† Electronic supplementary information (ESI) available. See DOI: 10.1039/d2ra00920j

As for the rheological, thermal stability, and textural properties of oleogel, aside from gelators, oil is another key factor.[20] The oleogel can be made from nutrient-rich vegetable oils, such as those rich in mono and polyunsaturated fatty acids.[21] Walnut oil (WO) contains mainly unsaturated fatty acids, such as oleic acid (14.9–28.7%), linoleic acid (50.6–66.6%), and linolenic acid (9.2–16.4%).[22] These unsaturated fats play an vital role in regulating blood lipids, cleaning blood clots, and improving body immunity.[23–25] In addition, WO is rich in micronutrients, such as phytosterols, squalene, polyphenols, and tocopherols, and its flavonoid content is significantly higher than that of peanut oil, corn oil, and other common vegetable oils. It is currently mainly consumed as a health oil and low-temperature cooking oil, but deep processing remains lacking.[26] WO possesses high biological activities, including good nutritional function and antioxidant property. Therefore, it is a new kind of oleogel material with development potential.

This study aimed to prepare complex oleogels and explore the influence of different water contents on the properties and structure of oleogels in an oil–wax–starch mixture. The oleogels were formed by mixing the oil and water phases. To evaluate the potential applicability of oleogels in food, we evaluated the binding ability of oleogels. In addition, the rheology, thermodynamics, and microstructure of the oleogels were characterized. This study aimed to provide a reference for expanding the application range of WO and transforming the inherent morphology of WO. The effects of mixed components on the three-dimensional network structure and gel mechanism of oleogels are discussed to provide technical reference and theoretical basis for the development of the low-oil oleogel industry.

2. Materials and methods

2.1 Materials

Candelilla wax (CW, food grade, 98%) and potato starch (PS, 11.2% moisture and 20.3% amylose content) were provided by Macklin Biochemical Co., Ltd. (Shanghai, China). Walnut oil (WO, unsaturated fatty acid content ≥92%) was purchased from Haoyouduo Supermarket, Shaanxi, China. All other reagents and chemicals used for analysis were analytical grade.

2.2 Preparation of the oleogels

Briefly, CW (4%) was added to WO under heating at 80 °C for 15 min to melt all the wax and form the dispersed oil phase. PS (2%) was dispersed in deionized water, and then heated and stirred in a water bath (Midea Inc., Beijing, China) for 5 min to form a disperse aqueous phase. The oil and water phases were mixed (9 : 1; 8 : 2; 7 : 3; 6 : 4; 5 : 5) and stirred (Model EM300T, Labotech Inc., Germany) at 80 °C for 15 min to fully mix the emulsion evenly.

An AH-2010 high-pressure homogenizer (Antrox nanotechnology (Suzhou) Co., Ltd, China) was used to process the pre-emulsion by pressurizing it twice (100/500 bar). After homogenization, the resulting emulsion was cooled to room temperature (20–25 °C). The cured emulsion was then stored at 4 °C

before characterization. These conditions were determined after preliminary trials. The schematic diagram for oleogel preparation is shown in Fig. S1.†

2.3 Textural characteristics

The firmness of the emulsions was analyzed using a TA.XT PLUS/50 texture analyzer (Stable Micro Systems Ltd., Surrey, UK). The oleogel was prepared and stored in a 30 mm glass cylindrical container for testing. A flat-ended cylindrical probe with a radius of 5 mm was inserted into the sample container to a 10 mm depth, and the velocity of the probe was set to 1.0 mm s^{-1}. The sample was tested at a rate of 1.0 mm s^{-1}. The trigger force was set at 3.0, and the trigger type was set to auto. Each trigger interval was 5.0 s. All samples were measured five times and subsequently averaged.

2.4 Oil loss rate (OLR) determination

The fat systems were stored at 4 °C overnight for balancing and stabilization. The OLR of the oleogel was determined by centrifugation. About 1–1.5 g of oleogel sample was poured into a centrifuge tube. Then, the sample was centrifuged at 10 610×g for 15 min, and then the tubes were let stand for 15 min. The purpose of the filter paper was to absorb the excess oil. The calculation formula for OLR is as follows:

$$OLR = \frac{(m_1 - m)(m_2 - m)}{(m_1 - m)} \times 100\%,$$

where m represents the quality of the empty tube, m_1 represents the quality of the tube with the initial sample, and m_2 stands for the final sample quality.

2.5 Rheological measurements

Rheology measurements were carried out by using a MCR 301 rotary rheometer (Anton Paar, Graz, Austria). The experiment was performed using a 40 mm aluminum Pearl flat plate geometry and a gap size of 1000 mm. Before analysis, all samples were prepared and decomposed completely. All rheological measurements were performed under room temperature. Oleogel strain scan tests were performed under a strain amplitude of 0.01–100% and frequency of 1 Hz. Frequency sweep tests were performed at the frequency range of 0.1–100 Hz and strain of 0.01% for oleogels. Flow measurements were operated at a shear rate range of 0.1–100 s^{-1} for oleogels.

2.6 Differential scanning calorimetry

The thermal properties of different oleogels were determined using a differential scanning calorimeter (DSC) Q2000 (Waters, Shanghai, China). The 5.0 mg oleogel sample was placed in an aluminum plate, and an empty plate was selected as a control. The sample heating temperature was from 20 °C to 60 °C at 10 °C min^{-1}, followed by cooling to −40 °C, at which the sample was kept for 5 min to crystallize completely, and then finally heated to 25 °C. The heat change rate for this process was 10 °C min^{-1}.

DSC STARe software was used to calculate the initial temperature, maximum value, enthalpy of melting and enthalpy of crystallization of each peak. Each experiment was repeated three times.

2.7 FTIR analysis

Infrared spectrometry was performed on samples using a VERTEX 70/70v infrared spectrometer (Bruker GmbH, Karlsruhe, Germany). For PS, infrared spectroscopy analysis was performed using the tableting method. The spectral information of oleogels and pure oil samples were collected using attenuated total reflection infrared spectrum technology. The spectra were scanned from 4000 cm^{-1} to 400 cm^{-1}, with an accumulation of 16 scans at a resolution of 4 cm^{-1}.

2.8 XRD analysis

XRD results were obtained by X-ray diffractometer (D8 ADVANCE A25 Bruker, Germany). Cu radiation ($\lambda = 1.5458$ Å) was used as the X-ray source and operated at 40 kV and 40 mA. The samples were analyzed in the diffraction angle range of 5–60° (2θ) and a rate of 2° min^{-1} step. The oleogel sample was carefully placed in the sample holder, which contained a groove 20 mm wide and 1 mm deep. The experiment was conducted at room temperature.

2.9 Microstructure analysis

The microstructure of the samples was studied using a Leica DM5000 B microscope (Leica Microsystems, Germany) with a color camera (Leica MC330 CCD). The oleogel samples were prepared on the center of a glass slide and then gently covered by a coverslip. After a night of cold storage, the samples were observed under 20× magnification and a polarizing microscope.

2.10 Statistical analysis

All analyses were conducted at least in triplicate. The data were presented as mean ± standard deviation. A significance level of $p < 0.05$ was set for the one-way analysis of variance (ANOVA) followed by Tukey's test. The XRD data were analyzed by USING MDI Jade 6 software (Materials Data Inc., Livermore, USA). Each FTIR spectrum was analyzed by the software OMNIC (Thermo, v7.3).

3. Results and discussion

3.1 Texture and OLR analysis

The self-assembly properties of wax and starch gels are the main reason for oleogel formation. The purpose of adding CW to the oil phase was to steady the oil–water interface and solidify the samples. PS has the functions of emulsification and thickening. It was arranged in order around the oil–water interface to form the interface film, allowing the oil drops to distribute well. The impacts of oil-to-water ratio on the hardness and OLR rate of the oleogel were determined by physical property analyzer and centrifugal method. The results are shown in Fig. 1.
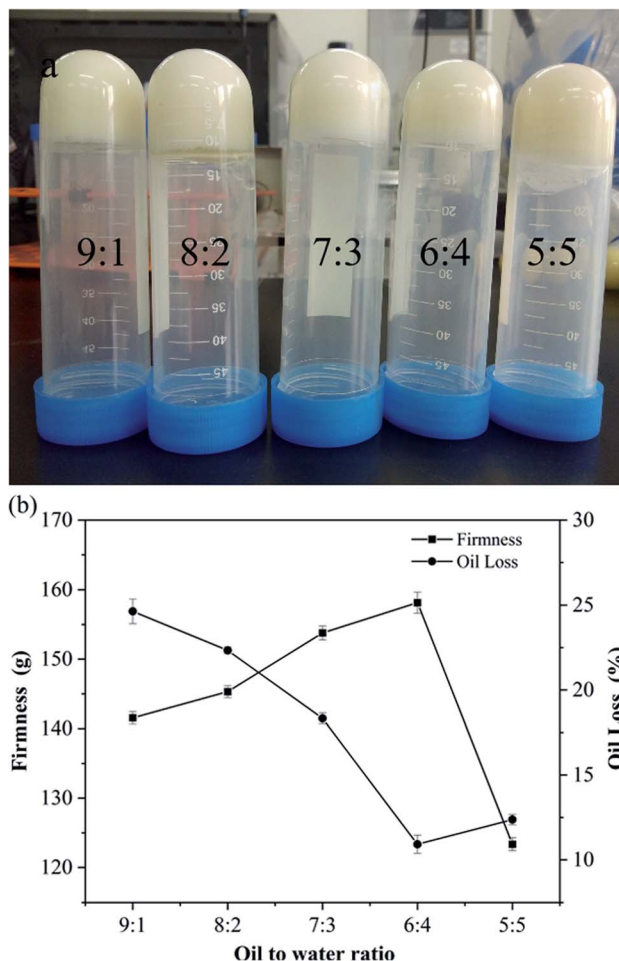

Fig. 1 (a) Oleogel oil-to-water ratios, (b) hardness and oil loss rate of oleogels.

The hardness of oleogels increased first and then decreased with an increase in water content, whereas the OLR rate of oleogels showed an opposite trend. When the ratio of oil-to-water was 6 : 4 (39%), the maximum hardness of oleogel was 158 g, and the lowest OLR rate was 10.91%, forming a relatively stable gel structure. With the increase of water content, the oleogel system became unstable, and oil–water stratification appeared (Fig. 1a). This finding contradicted previous results[27] possibly because the addition of water affects the gel system, and a proper moisture content could produce an optimal oleogel system. The specific interactions among starch, wax, and oil need further exploration.

3.2 Rheology analyses

To obtain more information about the effect of water content on the structure and properties of the oleogel network, we carried out rheological measurements. With the presence of external force, oleogels were deformed and became elastic. When the force disappeared, the oleogels presented viscous and fluidity features.[28]

Fig. 2a shows the amplitude scanning information of the oleogel samples with different oil-to-water ratios. G'' refers to
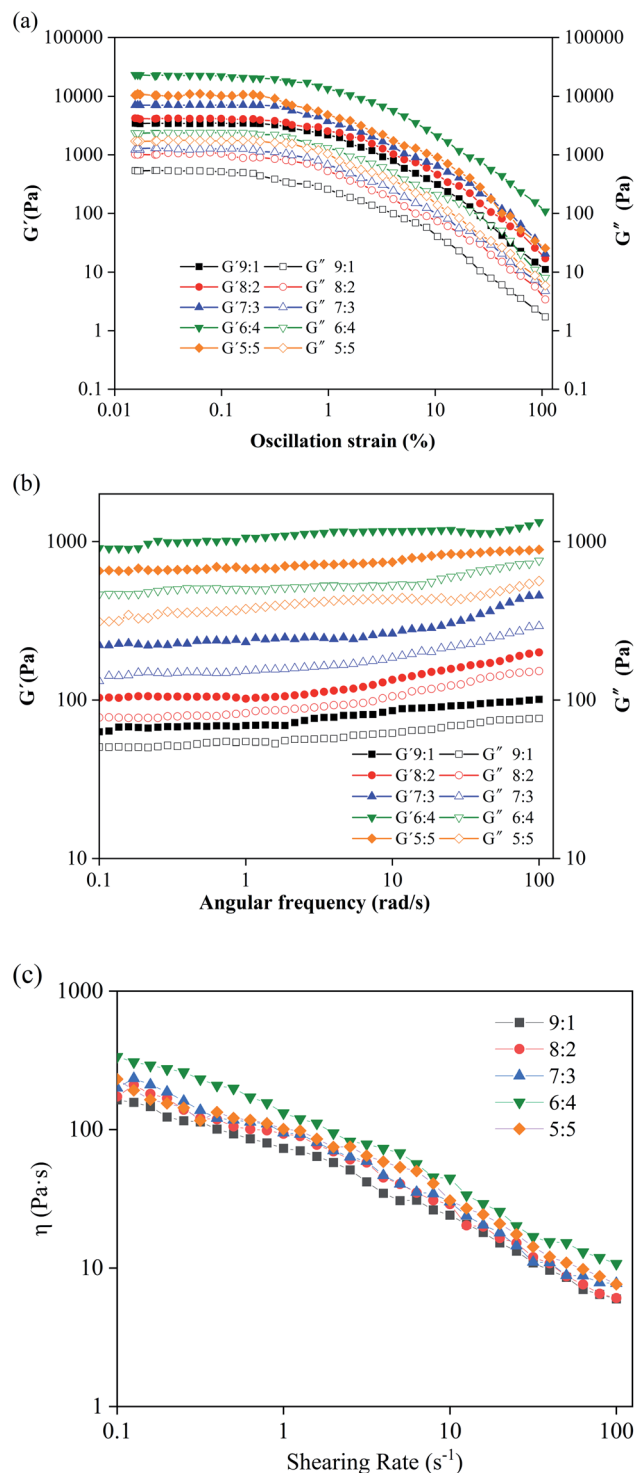
(a)

(b)

(c)

Fig. 2 Rheological behavior of oleogels with different oil-to-water ratios. (a) Amplitude sweep, (b) frequency sweep, and (c) flow measurement curves.

the solid/elastic character of oleogels: the more resistant the oleogel is to deformation, the higher the G'' value.[29] As can be seen from Fig. 2a, in the linear viscoelastic region, all oleogels showed a dominant 'solid' behavior ($G' > G''$); especially, when the ratio of oil to water was 6 : 4, G' and G'' reached the

maximum. This finding was obtained possibly because the addition of starch and water enhanced the intermolecular region in the noncovalent bond.[30] Under this condition, it formed more self-assembled structures of the oleogel. This made the oleogels become more stable and harder to deform.[29]

To evaluate additional information on oleogel samples, frequency scanning was performed. Results showed that the values of G' and G'' had a low frequency dependence, and the G' values were always greater than the corresponding G'' and independent of frequency (Fig. 2b), which is characteristic of the gel and consistent with their strain scan results (Fig. 2a). Therefore, water can induce the flow of droplets to form solidified droplets and promote interactions between droplets to form a network. Interestingly, none of the curves intersected ($G' = G''$), which indicated that the oleogels were not converted from gel to higher-frequency sol.[5]

The apparent viscosity of the oleogels increased with the increase of water content, and all samples exhibited significant shear thinning behavior (Fig. 2c), indicating that the shear process would lead to disintegration of the network in the oleogels.[31] At the initial stage of shear, large shear stress was needed to destroy the gel network structure, and then increasing starch molecules changed from the initial network structure to a directional flow, showing a "liquid" behavior, resulting in shear stress tending to smooth.

The curve of shear stress τ and shear rate was fitted using power law equation *via* regression. The Herschel–Bulkley model can be expressed as $\tau = \tau_0 + K\gamma^n$, where τ is the shear stress/Pa, τ_0 stands for the yield stress/Pa, K is the consistency coefficient/ (Pa s), γ is the shear velocity/s^{-1}, and n represents the flow index. The Herschel–Bulkley model parameters of oleogels with different oil-to-water ratios are shown in Table S1.†

For all oleogel samples, the correlation coefficient R^2 was high (0.965–0.997), indicating that the flow behavior of oleogels obeyed the power law equation. The value of K is related to the thickening ability. When K increases, the thickening ability of the emulsion also increases. When the oil-to-water ratio was 5 : 5, the fitting degree (~0.975) was not very high, and the previous rheological behavior was consistent with this finding. This finding was obtained possibly because of the formation of large and irregular droplets in the oleogel (Fig S3e†) and the existence of oil–water stratification. N is the fluidity characteristic index, which indicates the degree of difference between non-Newtonian and Newtonian fluids. Based on Table S1,† the non-Newtonian exponent n of the oleogel was less than 1 and in the range of 0.14–0.39, which indicated that it is a pseudoplastic fluid, and this result is consistent with the shear thinning result from the flow curve (Fig. 2c). The smaller the n was (the farther away from the Newton type it was), the easier the liquid undergoes shear thinning, and the greater the pseudoplasticity. When the oil-to-water was 6 : 4 (39%), the value of K was maximum (21.90), and the value of n was minimum (0.12). According to the results of rheology analysis, PS-CW-oil formed a type of composite oleogel, which is further proved in the following results.

3.3 DSC analysis

The crystallization behavior of CW, PS and oleogels was determined by DSC. Fig. S2† shows the DSC thermograms of the oleaginous samples of CW, PS and different oil-to-water ratios. It can be seen from Fig. S2† that the crystallization curve is above the horizontal axis and the melting curve is below. Broad peaks appeared in the thermograms of PS at 68 °C. The crystallization and melting temperatures of CW are 57.14 and 62.38 °C, respectively. The two main endothermic and exothermic peaks were observed during cooling and melting of the oleogels (Fig. S2c†). The addition of starch and distilled water affected the DSC curves of oleogels. With the increase in water content, the exothermic peak moved to a lower temperature direction, whereas the endothermic peak moved to a higher temperature direction. As shown in Fig. S2† and Table 1, the crystallization and melting points of the oleogel samples were distributed in the range of −22.71 °C to −14.86 °C and −1.54 °C to −1.41 °C, respectively. The value of ΔH increased from 19.11 w/g to 91.68 w/g, and increasing impurity peaks appeared in the crystallization peaks, indicating that the water content had a significant effect on the oleogel. The formation of a tighter, more regular oleogel system was associated with an increase in the concentration of water and starch. Differences were observed among the results for the peaks of carnauba wax/adipate oleogel samples at the melting temperature of 80 °C,[32] possibly because of the influence of water on the ΔH value in the complex system. The results showed a liquid-to-solid phase transition in the oleogels, and water and starch may be significant in the structure of the oleogels.

3.4 Changes in FTIR spectra

Fig. 3 shows the FTIR spectra of CW, PS, WO, and walnut oleogels prepared under different oil-to-water ratios.

From Fig. 3(a), the broad band at approximately 3304 cm^{-1} corresponds to the stretching vibration of O–H in starch, and the absorption peak at 2935 cm^{-1} may be attributed to CH–stretching vibration. The peak at 1641 cm^{-1} indicates the
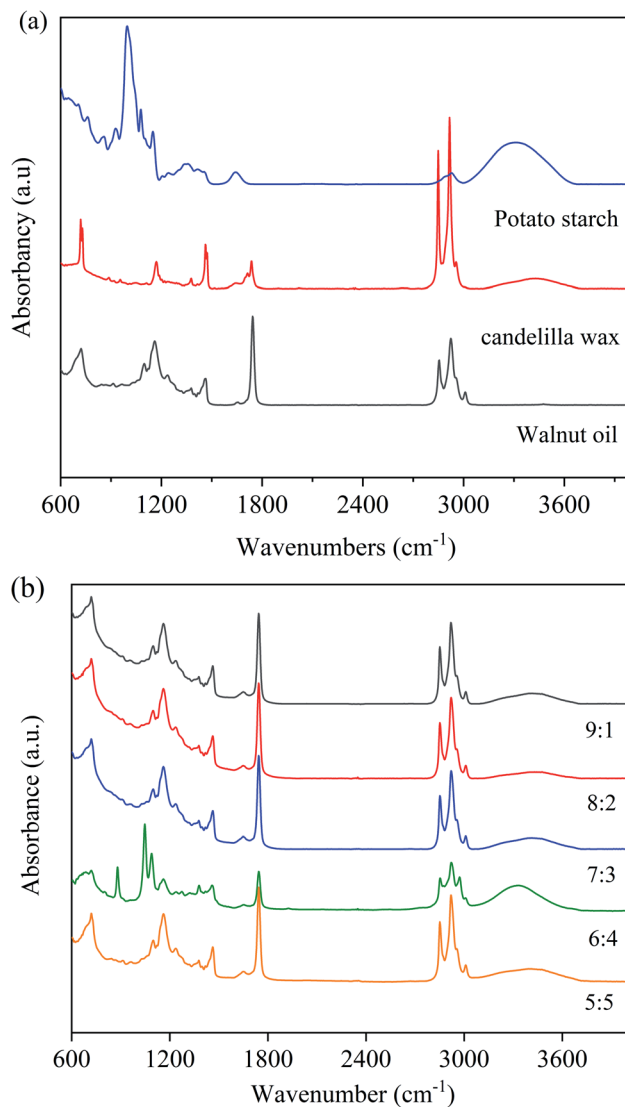
Fig. 3 FTIR spectra of walnut oleogels prepared at different oil-to-water ratios ((a): PS, CW, WO; (b): oleogels).

Table 1 Cooling and heating analysis results of oleogel samples by differential scanning calorimetry[a]

Sample	T_{on}/°C	T_p/°C	T_{end}/°C	T_g/°C	ΔH/w/g
Crystallization					
9 : 1	−13.9 ± 0.33e	−14.86 ± 0.35c	−22.76 ± 0.44e	−22.04 ± 0.23a	19.11 ± 1.12e
8 : 2	−15.98 ± 0.29d	−19.28 ± 0.45b	−23.53 ± 0.37d	−16.58 ± 0.12d	30.31 ± 1.98c
7 : 3	−18.93 ± 0.24b	−21.27 ± 0.56ab	−26.24 ± 0.41c	−22.00 ± 0.55a	47.16 ± 2.65b
6 : 4	−19.04 ± 0.37a	−22.71 ± 0.20a	−27.58 ± 0.39b	−19.31 ± 0.46b	59.10 ± 3.10a
5 : 5	−18.17 ± 0.43c	−18.995 ± 0.32b	−28.67 ± 0.36a	−17.29 ± 0.32c	20.0 ± 1.47d
Melting					
9 : 1	−6.57 ± 0.11b	−1.54 ± 0.02a	3.61 ± 0.21c	−1.49 ± 0.11a	47.30 ± 2.79e
8 : 2	−5.47 ± 0.17d	−1.41 ± 0.10a	3.94 ± 0.22b	−1.39 ± 0.45c	64.05 ± 2.55d
7 : 3	−5.47 ± 0.14d	−1.51 ± 0.04a	4.38 ± 0.27a	−1.48 ± 0.26ab	71.97 ± 2.94c
6 : 4	−6.78 ± 0.20a	−1.49 ± 0.09a	3.18 ± 0.30d	−1.46 ± 0.37b	83.99 ± 3.13b
5 : 5	−6.02 ± 0.25c	−1.46 ± 0.07a	3.18 ± 0.41d	−1.45 ± 0.04bc	91.68 ± 3.45a

[a] Different letters indicate significant differences between oleogel samples at $p < 0.05$. Crystallization and melting onset temperature (T_{on}), peak temperature (T_p), terminal temperature (T_{end}), and enthalpy change (ΔH) of different oleogel samples.

aldehyde group vibration peak of starch. The absorption peak at 1000–1300 cm^{-1} was in touch with the stretching vibration peak of the C–O–C bond.[33] Based on the spectra of WO and CW, C–H stretching vibration peaks of unsaturated carbon chains were observed at 3008 cm^{-1}, while anti-symmetric and symmetric stretching vibration peaks of saturated carbon chains were observed at 2924 and 2854 cm^{-1}. At 1745 cm^{-1}, a large spike associated with C=O stretching was found, and these peaks are obtained from the WO. The peaks at 1452 and 1381 cm^{-1} confirmed the presence of C–H bending of methyl and methylene groups. The band at 1125–1095 cm^{-1} is associated with the C–O stretching vibration peak and the methylene C–H bending vibration peak in triglycerides.[34]

The FTIR spectra of walnut oleogels are shown in Fig. 3(b). The oleogels exhibit weak and wide O–H absorption from 3650–3200 cm^{-1}, and a strong absorption peak at an oil-to-water ratio of 6 : 4. A wide spectrum peak appeared in PS, indicating that intramolecular or intermolecular hydrogen bonds exist in the oleogels originated from starch.[34] Hydrogen bonding is very important for forming the oleogel network.[35] The semi-crystalline structure of PS mainly comes from the hydrogen-bonded polymer entanglement. Oil droplets are trapped in the oleogel because of the hydrogen bonding between starch and water. In the study of ethyl cellulose oleogels, hydrogen bonds between polymer chains were found to be responsible for forming a network connecting liquid oils.[36] The significant absorption peaks at 3,008, 2,924, 2,854, and 1745 cm^{-1} were associated with WO and CW. These peaks were significantly lower in strength than those under other conditions, indicating that the oil droplets were firmly trapped and tightly bound. In the sample with 6 : 4 ratio, a peak associated with (CH$_2$)n bending was observed at 879 cm^{-1}, and this peak may be related to the presence of starch. By comparing the FTIR spectra of the components, we found that the absorption of the oleogels was mainly due to the functional groups of starch and WO; similar results were found in gels made from beeswax.[37]

3.5 X-ray diffraction spectrum

To further study the crystal morphology of the oleogels, we conducted XRD analysis. In Fig. 4, the XRD patterns of CW, PS, and oleogels are provided as a reference.

For a comprehensive comparison of the changes in XRD characteristics, we set the XRD patterns of CW and PS as controls. In Fig. 4(a), two peaks were discovered at 3.72 and 4.0 Å in CW. For PS, a wide peak was observed at $2\theta = 20.0$ Å (Fig. 4b). These results supported the finding that most of the carbohydrates were amorphous.[38] As shown in Fig. 4(c), a broad peak at 4.41 Å can be discovered in the oleogel sample, which is related to the main amorphous structure. The finding indicated the presence of a liquid triglyceride in the gel. A sharp peak at 4.12 Å and a weak peak at 3.72 Å were observed, indicating the presence of β-crystals with an orthorhombic perpendicular (O⊥) subcellar structure.[39,40] The β-polycrystals have an orthogonal-to-vertical subcellular structure and a uniform and creamy texture, which is most suitable for commercial margarines and daubs. The oleogels had a broad peak at around 20 Å,
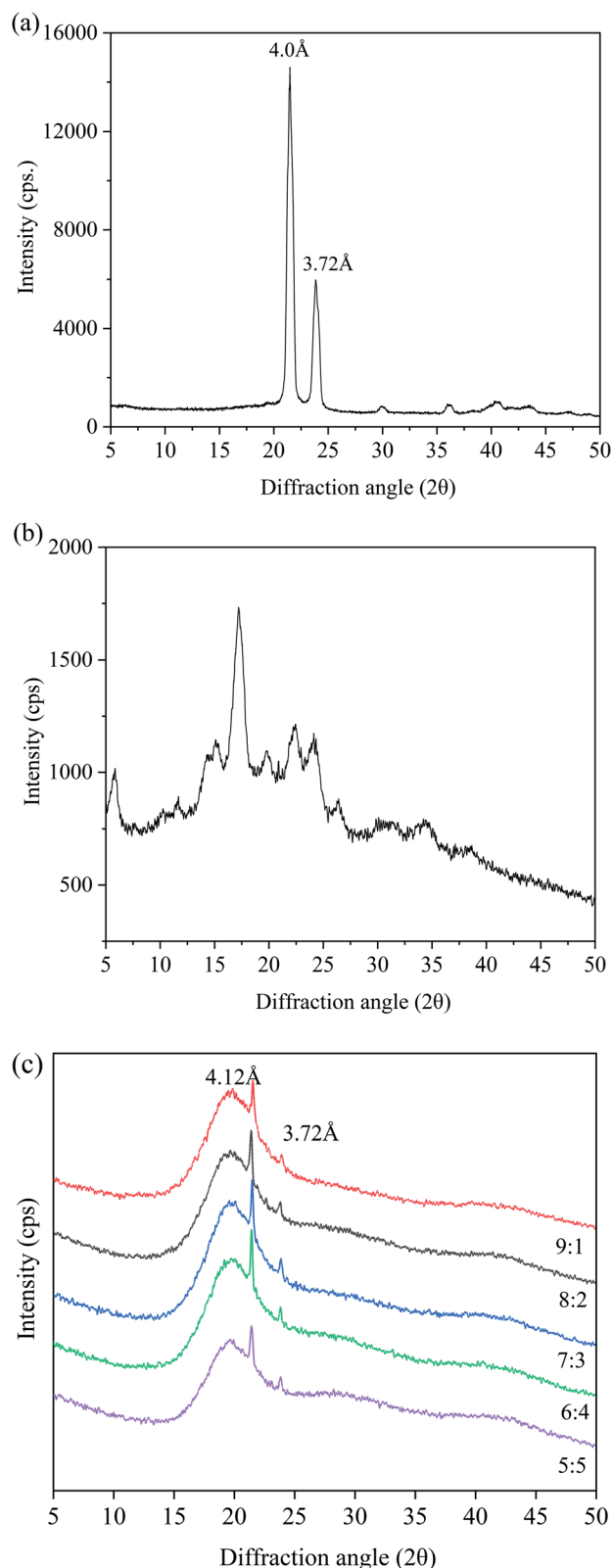

Fig. 4 XRD images of oleogels with different oil/water ratios. ((a): CW; (b): PS; (c): different oil/water ratios).

because of the starch molecular chain in the oleogel structure of the extension and winding caused by the conformational change.[41] Starch molecules formed a protective layer around the

oil droplets and interact to form an ordered structure. There were no obvious differences among XRD patterns of the oleogels with different water contents. When the oil-to-water ratio was 6 : 4, peak strength was largest, accounting for the maximum hardness and lowest OLR rate. Overall, the results of XRD patterns indicated that all the oleogels were regularly structured and retained liquid oils effectively.

3.6 Microstructure of oleogels

3.6.1 Light microscope. The size and shape of the droplets in the walnut oleogel are shown in Fig. S3.†

As shown in Fig. S3(a)–(e),† with the increase of water content, the droplets in the oleogel gradually grew larger, and the droplet morphology gradually changed from spherical to non-spherical.[42] When the oil-to-water ratio was 9 : 1, a slight reflective phenomenon was observed on the surface, which is consistent with the observed phenomenon in Fig. 1(a). Moreover, the droplets became more compact, especially when the oil-to-water ratio was 6 : 4 (Fig. S3d†); all the droplets seemed to interact and connect, in accordance with the results of FTIR. Similar gelation behavior of starch nanocrystals stabilized as high-in-phase emulsions was reported in micrographs.[41] When the oil–water ratio was 5 : 5, the particle distribution was larger, indicating that the droplets may form large clusters and show obvious droplet flocculation and coalescence. Based on Fig. S3,† the oleogel droplet size was slightly more dispersed in an oil-to-water ratio of 9 : 1. When the oil-to-water ratio was 6 : 4, the droplet distribution was more uniform, forming a more stable gel structure.

3.6.2 Polarized light microscopy. The microstructure of oleogels under different oil–water ratios was observed under polarized light. These crystals were seen as dense crystals,[43] consistent with previous studies.[29] As shown in Fig. 5, CW crystals appeared needle-like and fibriform,[29] which is a key factor to form ideal oleogels[44] capable of trapping large amounts of oil in crystalline structures. In Fig. 5(a–d), with the increase of water content, these long fibers tended to form larger networks. As a result, the space for crystal movement was reduced, and the network structure was more closely constructed.[45] When the oil/water ratio was 6 : 4, we can see that the crystal net was more uniform and denser. These crystals interacted to form tight three-dimensional networks and powerful gel properties, while larger and irregularly shaped crystals interspersed with crystal aggregates[46] were observed at an oil–water ratio of 5 : 5.

4. Conclusion

In summary, a walnut oleogel with good properties was prepared by mixing oil and water phases *via* two-step method, and we evaluated the effects of water content on the physical and microscopic properties of oleogels. Walnut oleogels had good performance when the oil-to-water ratio was 39%. The hardness was 158 g, and the OLR rate was 10.91%. According to infrared analysis, material components interacted intramolecularly or extramolecularly to form a three-dimensional network structure to fix the liquid oil and further form a stable gel structure. XRD analysis showed that the walnut oleogel had β-shaped crystals with a uniform and creamy texture, which is best suited to commercial margarines and spreads. With an increase in water content, the size and quantity of the crystals increased. Polarizing microscope images showed that all the oil gels had more visible crystals. Moreover, intramolecular or
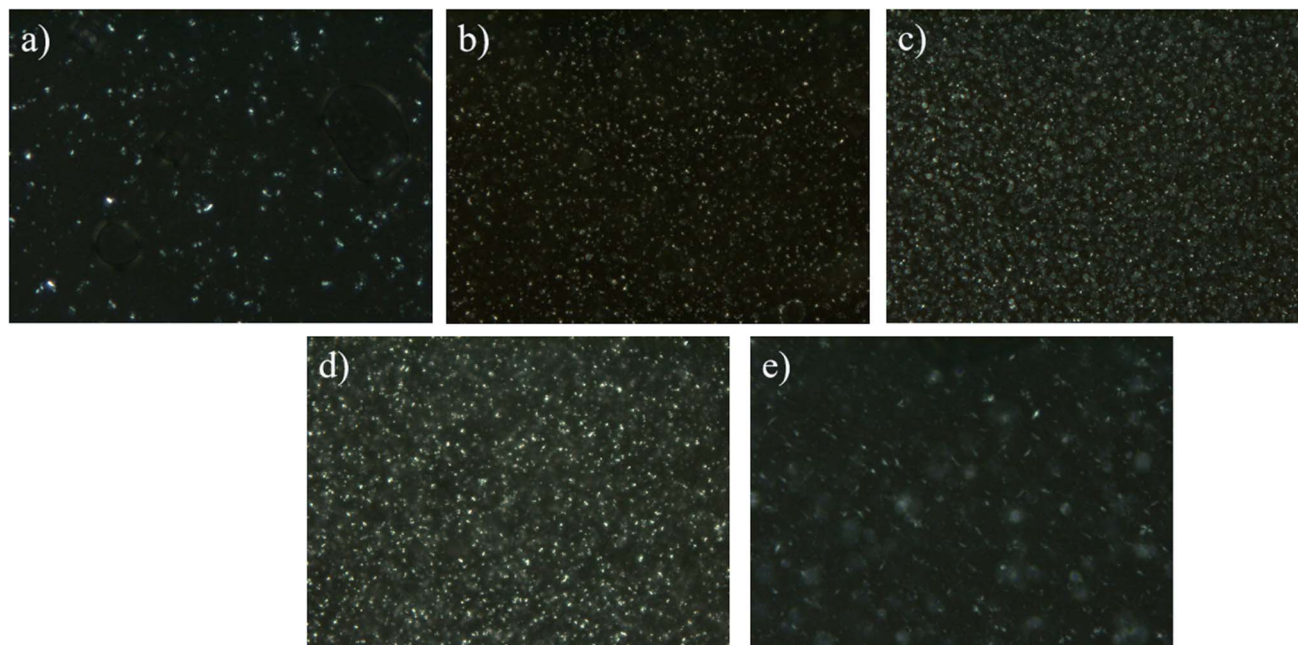

Fig. 5 Polarized light microscopy of oleogels prepared under different oil/water ratios at 20× magnification. ((a): 9 : 1; (b): 8 : 2; (c): 7 : 3; (d): 6 : 4; (e): 5 : 5).

intermolecular hydrogen bonds in the oleogels caused the droplets to bind more tightly and form a more compact network structure, further promoting the gelation. In general, these results clearly demonstrated the influence of water content on the interaction of walnut oleogel mixing systems. The information provided in this study provides a basis for the adequate dispersion of hydrophilic compounds in oil or oil-based foods. Future studies may examine the effect of water content on the oxidative stability of oleogels.

Abbreviations

CW	Candelilla wax
WO	Walnut oil
PS	Potato starch
OLR	Oil loss rate
DSC	Differential scanning calorimetry
XRD	X-ray powder diffraction
T_{on}	Onset temperature
T_p	Peak temperature
T_{end}	Terminal temperature
ΔH	Enthalpy change;
G'	Storage modulus
G''	Loss modulus
η	Complex viscosity
ω	Angular frequency

Conflicts of interest

The authors declare that they have no known competing financial interests or personal relationships that could have appeared to influence the work reported in this paper.

Acknowledgements

Notes and references

1 I. Tavernier, C. D. Doan, V. Davy, S. Danthine, T. Rimaux and K. Dewettinck, *RSC Adv.*, 2017, 7, 12113–12125.
2 M. Sintang, S. Danthine, I. Tavernier, D. V. D. Walle and K. Dewettinck, *Food Hydrocolloids*, 2021, **115**, 106623.
3 S. Z. Luo, X. F. Hu, Y. J. Jia, L. H. Pan, Z. Zheng, Y. Y. Zhao, D. D. Mu, X. Y. Zhong and S. T. Jiang, *Food Hydrocolloids*, 2019, **95**, 76–87.
4 S. Stender, A. Astrup and J. Dyerberg, *BMJ Open*, 2012, **2**, 13.
5 A. R. Patel and K. Dewettinck, *Food Funct.*, 2016, 7, 20–29.
6 M. García-Andrade, R. F. González-Laredo, N. E. Rocha-Guzmán, W. Rosas-Flores and J. A. Gallegos-Infante, *Rev. Mex. Ing. Quim.*, 2020, **19**, 953–968.
7 A. G. Marangoni, *J. Am. Oil Chem. Soc.*, 2012, **89**, 749–780.

8 K. Abdolmaleki, L. Alizadeh, K. Nayebzadeh, S. Hosseini and R. Shahin, *J. Texture Stud.*, 2020, **52**, 290–299.
9 C. Blach, A. J. Gravelle, F. Peyronel, J. Weiss, S. Barbut and A. G. Marangoni, *RSC Adv.*, 2016, **6**, 81151–81163.
10 A. R. Patel, N. Cludts, M. D. B. Sintang, A. Lesaffer and K. Dewettinck, *Food Funct.*, 2014, **5**, 2833–2841.
11 K. Silva, A. I. Bourbon, L. Pastrana and A. Sato, *Food Res. Int.*, 2021, **141**, 110059.
12 K. Rehman, M. C. I. M. Amin and M. H. f. Zulfakar, *J. Oleo Sci.*, 2014, **63**, 961–970.
13 Y. R. Tang and S. Ghosh, *RSC Adv.*, 2021, **11**, 25141–25157.
14 M. D. Bin Sintang, S. Danthine, A. Brown and D. Van, *Food Res. Int.*, 2017, **100**, 832–840.
15 A. R. Patel, N. Cludts, M. D. B. Sintang, A. Lesaffer and K. Dewettinck, *Food Funct.*, 2014, **5**, 2833–2841.
16 K. C. Maki, M. S. Reeves, M. L. Carson, M. P. Miller and D. M. Wilder, *Diabetes Technol. Ther.*, 2009, **11**, 119–125.
17 I. Tavernier, C. D. Doan, P. Van der Meeren, B. Heyman and K. Dewettinck, *Eur. J. Lipid Sci. Technol.*, 2018, **120**, 1700393.
18 E. Scholten, *Current Opinion in Food Science*, 2019, **27**, 36–42.
19 X. B. Zhai, L. I. Hong-Jun and H. E. Zhi-Fei, *Food Ferment. Ind.*, 2016, **42**, 49–56.
20 H. Pehlivanoglu, M. Demirci, O. S. Toker, N. Konar, S. Karasu and O. Sagdic, *Crit. Rev. Food Sci. Nutr.*, 2018, **58**, 1330–1341.
21 E. D. Co and A. G. Marangoni, *J. Am. Oil Chem. Soc.*, 2012, **89**, 749–780.
22 P. Gao, R. J. Liu, Q. Z. Jin and X. G. Wang, *LWT–Food Sci. Technol.*, 2021, **135**, 109958.
23 A. B. Awad and C. S. Fink, *J. Nutr.*, 2000, **130**, 2127–2130.
24 J. Yang, R. H. Liu and L. Halim, *LWT–Food Sci. Technol.*, 2009, **42**, 1–8.
25 F. Muradoglu, F. Balta and P. Battal, *Acta Physiol. Plant.*, 2010, **32**, 53–57.
26 B. Mert and T. A. Vilgis, *Food Hydrocolloids*, 2021, **119**, 106832.
27 C. Aurora, E. S. Paulo, P. Munekata, V. S. Maríaet, D. Rubénal and M. L. José, *Int. J. Food Sci. Technol.*, 2021, **56**, 6182–6191.
28 G. Fayaz, O. Polenghi, A. V. Cerne and S. Calligaris, *Int. J. Food Sci. Technol.*, 2020, **56**, 3633–3640.
29 C. D. Doan, D. Van de Walle, K. Dewettinck and A. R. Patel, *J. Am. Oil Chem. Soc.*, 2015, **92**, 801–811.
30 Y. Gao and S. Wu, *Food Funct.*, 2020, **11**, 7727–7735.
31 O. S. Toker, N. Konar, H. R. Pirouzian, S. Oba and O. Sagdic, *LWT–Food Sci. Technol.*, 2018, **87**, 177–185.
32 A. A. Khiabani, M. Tabibiazar, L. Roufegarinejad, H. Hamishehkar and A. Alizadeh, *Food Chem.*, 2020, **333**, 127446.
33 Q. Lu, D. Li and J. Jiang, *J. Agric. Food Chem.*, 2019, **59**, 13004–13011.
34 Z. Meng, K. Qi, Y. Guo, Y. Wang and Y. Liu, *Food Hydrocolloids*, 2018, **77**, 17–29.
35 M. OEguetcue, N. Arifoglu and E. Yilmaz, *Int. J. Food Sci. Technol.*, 2015, **50**, 404–412.
36 C. Liu, Z. Zheng, Y. Shi, Y. Zhang and Y. Liu, *Food Chem.*, 2021, **345**, 128811.

37 Z. Shariatinia and A. M. Jalali, *Int. J. Biol. Macromol.*, 2018, **115**, 194–220.

38 C. Liu, Z. Zheng, Z. Meng, X. Chai, C. Cao and Y. Liu, *LWT–Food Sci. Technol.*, 2019, **115**, 108446.

39 C. Liu, Z. Zheng, F. Zaaboul, C. Cao, X. Huang and Y. Liu, *Food Funct.*, 2019, **10**, 5413–5425.

40 Z. Shi, L. Cao, S. Kang, S. Jiang and M. Pang, *Int. J. Food Sci. Technol.*, 2021, **57**, 2003–2014.

41 T. Yang, J. Zheng, B. S. Zheng, F. Liu, S. Wang and C. H. Tang, *Food Hydrocolloids*, 2018, **82**, 230–238.

42 Y. Yao, H. Zhou, W. Liu, C. Li and S. Wang, *J. Oleo Sci.*, 2021, **70**, 135–143.

43 T. Lomonaco, D. B. Arellano and S. Martini, *Food Res. Int.*, 2019, **121**, 900–909.

44 P. Terech and R. G. Weiss, *Chem. Rev.*, 1997, **97**, 3133–3160.

45 K. Wijarnprecha, K. Aryusuk, P. Santiwattana, S. Son-waiet and D. Rousseau, *Food Res. Int.*, 2018, **112**, 199–208.

46 S. E. Lumor, B. H. Kim and C. C. Akoh, *J. Agric. Food Chem.*, 2008, **56**, 9294–9298.